pubs.acs.org/Biomac

Article

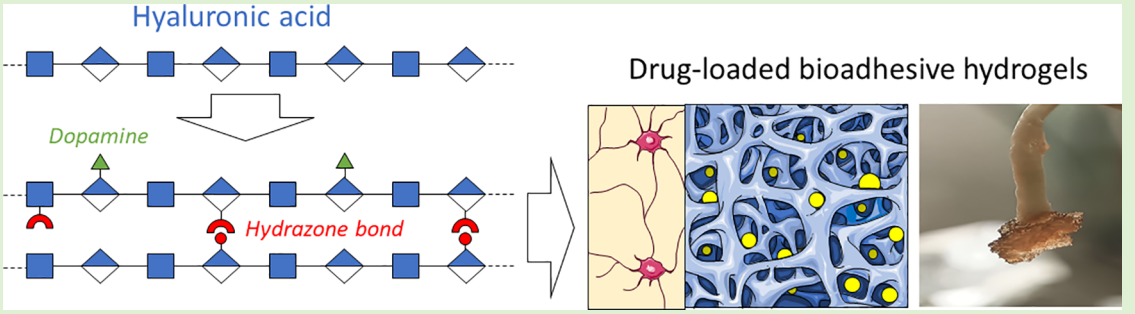
Bioadhesive Hyaluronic Acid-Based Hydrogels for Spinal Cord Injury

Diogo Duarte,[§] Cátia Correia,[§] Rui L. Reis, Iva Pashkuleva, Daniela Peixoto,* and Natália M. Alves*

Cite This: https://doi.org/10.1021/acs.biomac.3c01186

Read Online

ACCESS | Metrics & More | Article Recommendations | Supporting Information



ABSTRACT: Spinal cord injuries (SCI) have devastating physical, psychological, and psychosocial consequences for patients. One challenge of nerve tissue repair is the lack of a natural extracellular matrix (ECM) that guides the regenerating axons. Hyaluronic acid (HA) is a major ECM component and plays a fundamental role in facilitating lesion healing. Herein, we developed HA-based adhesive hydrogels by modification of HA with dopamine, a mussel-inspired compound with excellent adhesive properties in an aqueous environment. The hydrogels were loaded with the anti-inflammatory drug ibuprofen and the response of neuronal cells (SH-SY5Y) was evaluated in terms of viability, morphology, and adhesion. The obtained results suggested that the developed materials can bridge lesion gaps, guide axonal growth, and simultaneously act as a vehicle for the delivery of bioactive compounds.

1. INTRODUCTION

A spinal cord injury (SCI) is a vertebral column lesion that may result in temporary or irreversible neurologic dysfunction depending on the affected tissues. SCI symptoms include the loss of sensation, muscle weakness, paralysis, and loss of bowel or bladder control.[1,2] The injury can be a result of physical trauma or nontraumatic factors (e.g., diseases, infections, and tumors) and is classified into complete SCI, characterized by a total loss of sensory and motor function, and incomplete SCI, which leaves some degree of retained sensory or motor function.[1]

The complex anatomical and histological structure of the spinal cord makes SCI treatment difficult. The typical SCI treatments involve surgical interventions, such as early decompression of the injured cord, spinal realignment, and stabilization, removing disc pieces and ligament fragments from the injury site, and pharmacological drugs to treat some symptoms.[3] However, current therapies do not fully restore neural functions and delay only pathology progression. Therefore, the development of a new treatment to minimize apoptosis, oxidative stress, and inflammation, as well as regenerating axons is crucial for successful nerve tissue repair.[4,5]

Biomaterials can be used to bridge the lesion gap as well as to support nerve guidance.[6] Among biomaterials, hyaluronic acid (HA) has attracted great attention because it is a major extracellular matrix (ECM) component essential for neurogenesis and inflammation processes that are pivotal for tissue healing.[7] Hydrogels from HA have excellent biocompatibility and biodegradability, but their mechanical and tissue adhesion properties in an aqueous environment are poor. Previous studies have shown that these properties can be enhanced by HA modification with catechol groups without compromising HA biocompatibility and biodegradability.[8] Catechol-containing materials are inspired by mussel adhesive proteins and have demonstrated remarkably strong adhesion in different environments. The adhesion strength is preserved upon mechanical stress, e.g., stretching and twisting, mirroring the dynamic movements of the human body.[9,10] The functionalization of HA hydrogels with catechol groups has an effect beyond an enhanced adhesion; it promotes cell attachment, proliferation, and differentiation, having an effect that is similar to the action of the bioadhesive molecules from the extracellular matrix (ECM),[11] i.e., evokes a cellular response favorable for biomimetic and biomedical applications.

Based on these promising previous results, we developed adhesive hydrogels for SCI treatment by modification of HA

Received: October 31, 2023
Revised: February 2, 2024
Accepted: February 5, 2024

ACS Publications © XXXX American Chemical Society

with different molecular weights (MW) with dopamine. Because the controlled inflammation process is crucial for healing, we loaded the obtained hydrogels with an anti-inflammatory drug, ibuprofen, and studied the response of neuronal cells (SH-SY5Y) in terms of viability, morphology, and adhesion.

2. MATERIALS AND METHODS

2.1. Materials. HA with different MW: low (ref: HA20K) and medium (ref: HA500 K and HA700 K) were purchased from Lifecore. An ibuprofen pharmaceutical secondary standard was obtained from Supelco. All other reagents were purchased from Sigma-Aldrich if not stated.

2.2. Synthesis of Hyaluronic Acid Modified with Catechol Groups (HA-Cat). HA was chemically modified with catechol groups (HA-Cat) using a standard carbodiimide protocol as described by Lee and co-workers.[12] Briefly, 1 g of HA was dissolved in 100 mL of phosphate-buffered saline (PBS), and the pH was adjusted to 5.5 with an HCl aqueous solution. The solution was purged with nitrogen for 30 min. Then, 0.338 g of (3-(dimethylamino)propyl)-*N*′-ethyl-carbodiimide hydrochloride (EDC) and 0.474 g of dopamine hydrochloride were added. The pH was maintained at 5.5, and the reaction was performed for 2 h. Unreacted chemicals and urea byproducts were removed by extensive dialysis (membranes Spectra/Por 3, cutoff 3.5 kDa, Fisher Scientific) against osmotized water (OW). The final product was lyophilized and stored at −20 °C and protected from light. The functionalization was confirmed by ^{1}H NMR (Bruker Avance, 400 MHz) and ATR-FTIR (Shimadzu IRPrestige-21 FTIR spectrometer, 400−4000 cm^{-1}). The MW was obtained by gel permeation chromatography (GPC, Malvern Viscotek TDA 305 chromatograph).

2.3. Synthesis of HA-Cat-Aldehyde Derivative (HA-Cat-Al). HA-Cat was oxidized by adding $NaIO_4$. Briefly, 1 g of HA-Cat was dissolved in 100 mL of OW, and then 50 mL of an aqueous solution of $NaIO_4$ (2.67%) was added dropwise under stirring. The reaction was carried at room temperature, in the dark, for 30 min and stopped by adding ethylene glycol (1 mL).[13] Unreacted chemicals were removed by dialysis (cutoff 3.5 kDa) against OW. The final product, HA-Cat-Al, was freeze-dried and stored at −20 °C and protected from light. The success of the modification was confirmed by ^{1}H NMR and ATR-FTIR. The MW of the product was obtained by GPC. The degree of catechol substitution was determined by UV−vis spectrometry (Microplate Reader, Gen 5 2.01) using the absorbance band at 280 nm.

2.4. Synthesis of HA-Aldehyde Derivative (HA-Al). HA was oxidized to HA-Al by adding $NaIO_4$ using the same protocol as described above. The modification was confirmed by ^{1}H NMR and ATR-FTIR.

2.5. Modification of HA with Adipic Acid Dihydrazide (HA-ADH). HA-ADH was synthesized according to the procedure proposed by Luo et al.[14] Briefly, 1 g of HA was dissolved in 200 mL of OW, and then 18.3 g of ADH was added to this solution while stirring. The pH was adjusted to 5 by adding 0.1 N HCl. Next, 1.56 g of EDC was added and the mixture was stirred for 4 h at pH 5. The reaction was stopped by adding 0.1 N NaOH, raising the pH to 7. Unreacted chemicals were removed by dialysis (cutoff 3.5 kDa) against OW. The HA-ADH product was obtained by freeze-drying and then stored at −20 °C. The modification of HA was confirmed by ^{1}H NMR and ATR-FTIR. The MW was characterized by GPC.

2.6. Preparation of HA-Cat and HA Hydrogels. The HA-Cat and HA hydrogels were formed by a reaction between the terminal amine groups of HA-ADH and the aldehyde groups of HA-Cat-Al or HA-Al, respectively. Each HA derivative (HA-Cat-Al, HA-Al, and HA-ADH) was dissolved in PBS (pH 7.4) at a concentration of 24 mg/mL. Hydrazone cross-linked hydrogels were formed upon mixing equal volumes of the respective solutions (HA-Al and HA-ADH for the control; HA-Cat-Al and HA-ADH for the sample). The hydrogels were frozen at −80 °C for approximately 4 h and then freeze-dried for 24 h, obtaining a scaffold-like structure. These structures were hydrated in DMEM-F12 cell medium (Thermo Fisher Scientific) for further characterization and cellular assays.

2.7. Drug Loading into the Hydrogels. The anti-inflammatory drug ibuprofen was incorporated into the hydrogels at a concentration of 50 μM. Briefly, solutions of HA-Cat-Al and HA-ADH were prepared as described above. Then, 0.0103 mg of ibuprofen was added to HA-Cat-Al solution due to its low viscosity, which facilitates the drug's dissolution. The hydrogels were formed upon mixing 500 μL of this solution with 500 μL of the HA-ADH solution. The hydrogels were kept overnight at 4 °C, frozen at −80 °C and then freeze-dried.

It is worth noting that the freeze-drying process does not compromise the encapsulation of ibuprofen. This is attributed to ibuprofen's stability and nonvolatile nature, preventing it from subliming with water during freeze-drying. Consequently, ibuprofen remains effectively encapsulated within the matrix throughout the process.[15]

2.8. Stability Studies. The obtained hydrogels were freeze-dried, weighed, and soaked either in PBS or in a DMEM-F12 medium for 7 days at 37 °C in a CO_2 incubator. After this period, the hydrogels were removed from the solution, washed several times with ultrapure Milli-Q water, freeze-dried, and weighed. The weight loss was calculated using the following eq 1 (eq 1):

$$\text{weight loss} = \frac{W_i - W_f}{W_i} \times 100\% \quad (1)$$

where W_i is the initial weight of the dry sample and W_f is the final weight of the dry sample. All tests were performed in triplicate.

2.9. Assessment of Hydrogels' Mechanical Properties. The rheological measurements were performed using a Kinexus pro+ rheometer (Malvern Instruments) and Malvern's acquisition software rSpace. The plate−plate setup used in these trials was an upper geometry (8 mm of diameter) and a lower plate pedestal, both with stainless steel (316 grade) and with a rough finish. Oscillatory experiments were performed to study the viscoelastic properties of the hydrated freeze-dried hydrogels through the frequency sweep curves. The linear viscoelastic region was first assessed by strain sweep measurements (0.01−10%) using a constant frequency (1 Hz) at 37 °C. This region shows the range in which the oscillatory experiments can be carried out without imposing permanent deformation on the studied hydrogels. Then, the frequency sweep test was performed in the range of 0.1−100 rad/s at 37 °C.

Dynamic mechanical analysis (DMA) experiments were conducted by using a TRITEC 2000B instrument (Triton Technology) in the compressive mode. The thickness and diameter of each freeze-dried hydrogel were measured at three different points using a digital micrometer. Before DMA testing, the samples were soaked overnight in a DMEM-F12 cell medium to achieve equilibrium. Then, DMA scans of the freeze-dried hydrogel, immersed in DMEM-F12 medium, were recorded at 37 °C by using frequency cycles from 0.1 to 10 Hz. Three specimens were tested per condition.

The adhesive properties of the hydrated freeze-dried hydrogels were assessed using an *ex vivo* model, namely, porcine skin (*sus scrofa domesticus*, 12 weeks, male, 25 kg) donated by Life and Health Science Research Institute, University of Minho (Braga, Portugal). The assays were performed with Universal Mechanical Testing Equipment (INSTRON 5540) equipped with a load cell of 50 N, following a modified ASTM F2255 standard test method. Briefly, fresh porcine skin devoid of a fat layer was immersed in PBS solution (pH = 7.4) for 1 h before the test. Then, the porcine skin was cut into stripes measuring 3.5 cm in length and 1 cm in width. The hydrated freeze-dried hydrogels were placed between two stripes of porcine skin, resulting in a bonding area of 1.5 × 1 cm^2 for 2 h at 37 °C. Then, the two sample pieces were fixed between two grips positioned 2 cm in length axis. The crosshead speed of 5 mm/min was applied until the porcine skin detached. The test measured the applied force (load) and displacement (deformation) during the test using the test machine's sensors and data acquisition system. The lap-shear

https://doi.org/10.1021/acs.biomac.3c01186
Biomacromolecules XXXX, XXX, XXX−XXX

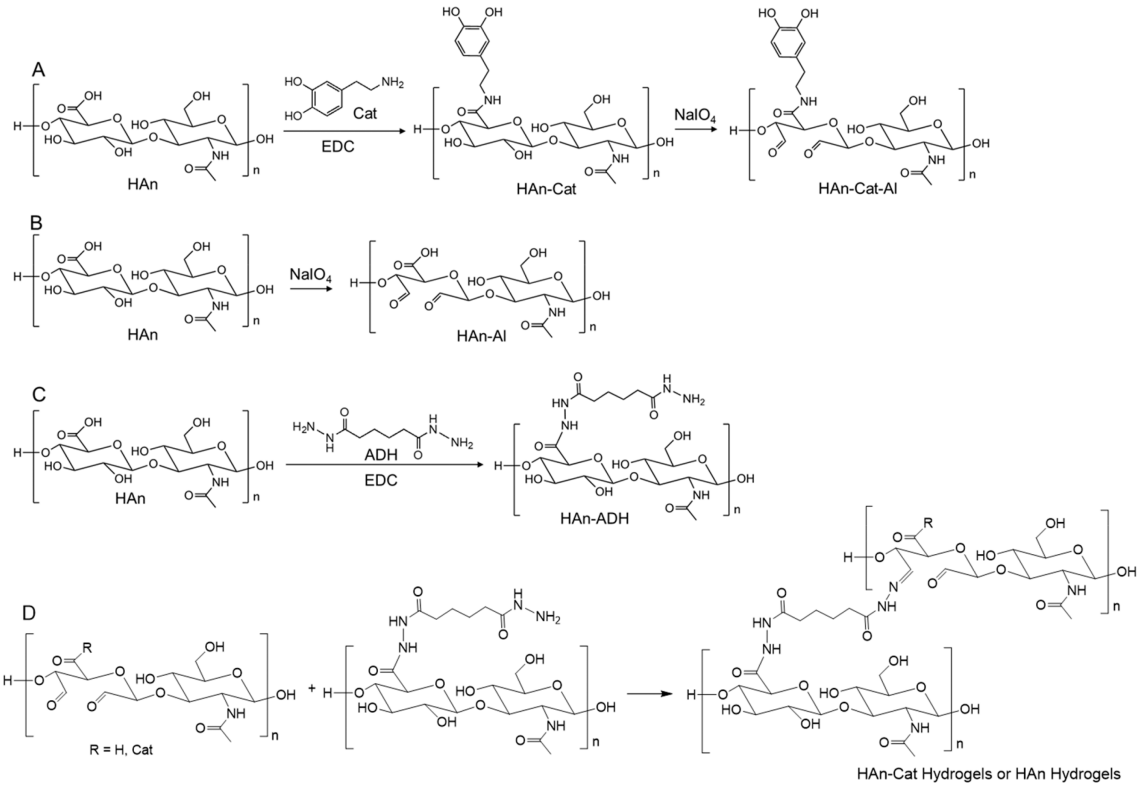


Figure 1. Schematic presentation of (A−C) hyaluronic acid (HA) modifications to obtain the components of the hydrogels (*n* represents the molecular weight of the HA) and (D) reaction between the obtained HA derivatives leading to the formation of hydrogels via a hydrazone bond.

adhesion was calculated by the ratio between the applied force and the area of adhesive overlap.[16,17]

2.10. Cellular Assays. The biocompatibility of the developed materials was assessed with a human neuroblastoma epithelial cell line (SH-SY5Y, Sigma-Aldrich) using passages 30 and 31. Cells were cultured in DMEM-F12 medium supplemented with 10% fetal bovine serum (FBS, Biorad) and 1% antibiotic−antimycotic solution under a humidified atmosphere of 5% CO_2 at 37 °C. The cell medium was changed every 2 days. When 80% of confluence was reached, the cells were washed with Dulbecco's phosphate buffered saline (DPBS, Biorad) and subsequently detached with 5 mL of trypLE express (Thermo Fisher Scientific) solution for 5 min at 37 °C. To inactivate the trypLE express, 10 mL of culture medium were added. The cells were centrifuged at 200*g* for 5 min, and the medium was removed. The obtained pellet was resuspended in a DMEM-F12 medium.

Before cell seeding, the hydrogels were UV sterilized for 1 h and washed with DMEM-F12 medium with 10% of antibiotic, followed by washing several times with DPBS and immersion in DMEM-F12 medium without FBS supplementation for 24 h. Then, 300 μL of cell suspension in DMEM-F12 (2×10^6 cells/mL) were added dropwise on the hydrogels and the tissue culture polystyrene (TCPS, control). The samples were incubated at 37 °C in a humidified atmosphere of 5% CO_2. After 4 h, a fresh culture medium was added to 2 mL of volume.

Live/Dead assays were performed to analyze hydrogels cytotoxicity. After 1, 3, and 7 days of culture, the medium was aspirated, and each hydrogel was immersed in 500 μL of DMEM-F12 medium supplemented with 1 μg of Calcein AM (2:1000, Thermo Fisher Scientific) and 0.5 μg of PI (1:1000, Thermo Fisher Scientific) for 30 min at dark. Subsequently, samples were rinsed with PBS and analyzed using an AiryScan 2 confocal microscope (LSM 980, Zeiss).

The arrangement of the cytoskeleton was observed by using fluorescent microscopy after histochemical staining. The culture medium was aspirated from cultures of 1, 3, and 7 days, and the samples were washed with PBS and then fixed in 4% paraformaldehyde (Thermo Fisher Scientific) for 30 min. Subsequently, the fixed samples were permeabilized with a solution of Triton X-100 (0.2% v/v in PBS) for 3 min, followed by immersion in bovine serum albumin (BSA, 3% w/v in PBS) for 1 h. After these steps, the samples were incubated with the primary antibody β-tubulin III (Abcam, 1:500 in 1% BSA) overnight at 4 °C, washed with PBS and incubated with a secondary antibody antirabbit AF 594 (1:500 in PBS, Life Technologies) and 4′,6-diamidino-2-phenylindole dilactate (DAPI, 1:1000 in PBS, Biotium Inc.) for 1 h at RT. Samples were extensively rinsed with PBS and analyzed using an AiryScan 2 confocal microscope (LSM 980, Zeiss).

The cytotoxicity of ibuprofen was assessed by studying the SH-SY5Y viability at different concentrations of ibuprofen in DMEM-F12 medium. According to previous studies, 100 μM of ibuprofen causes a significant reduction in cell viability.[6] Herein, the effect of ibuprofen on cell viability was assessed by indirect assays using 1 μM, 50 μM ibuprofen and a control condition without the drug. SH-SY5Y were seeded on 96-well plates at a density of 30000 cells per well. Medium (100 μL per well) without ibuprofen (control) or supplemented with 1 or 50 μM ibuprofen were added to the wells and incubated for 3 days. All assays were performed in triplicate.

Cultures after 1, 2, and 3 days were assessed for metabolic activity using an Alamar-Blue assay, viability using a live/dead assay, and morphology using immunohistochemistry. The Alamar-Blue assay was performed by removing the culture medium from the cultures at each time-point and adding a fresh medium supplemented with 10% Alamar-Blue reagent, followed by incubation at dark for 4h at 37 °C in a humidified atmosphere of 5% CO_2. Then, 100 μL of each solution was transferred to a 96-well black plate, and the fluorescence was measured at 590 nm emission wavelength and 530 nm excitation wavelength using a microplate reader (BIO-TEK instruments). The live/dead and immunohistochemistry were performed as described above. We encapsulated the determined optimal concentration of ibuprofen, which equated to 50 μM.

The freeze-dried hydrogels loaded with ibuprofen were sterilized using the same protocol described above and then hydrated with DMEM-F12 medium (2 h) before cell seeding. SH-SY5Y cells were

https://doi.org/10.1021/acs.biomac.3c01186
Biomacromolecules XXXX, XXX, XXX−XXX

seeded and characterized as described above for the nonloaded hydrogels.

2.11. Statistical Analysis. Statistical analysis was performed by GraphPad Prism software (version 8.0, GraphPad Software Inc.). A p-value < 0.05, corresponding to a minimum confidence interval of 95%, was accepted as a limit for statistical significance. The following symbols were used in the Results and Discussion: *p < 0.05, **p < 0.01, ***p < 0.001, ****p < 0.0001. Graphs denote statistically significant values, and the data are presented as mean ± standard error.

3. RESULTS AND DISCUSSION

3.1. HA Modification. HA with different MWs (calculated from GPC data: 37, 454, and 926 kDa, Figure S1) were modified with catechol groups by a reaction with dopamine in the presence of EDC (Figure 1A). The modification was confirmed by ^{1}H NMR (Figure S2) and ATR-FTIR (Figure S3) spectroscopy. ^{1}H NMR spectrum of HA-Cat shows the presence of aromatic protons from the catechol at δ = 6.7−7.4 ppm. The ATR-FTIR spectrum of HA-Cat exhibited bands and patterns similar to those observed in the HA spectrum. However, some signals in the HA-Cat spectrum, such as −OH and −NH peaks at 3270 cm^{-1}, were broader, indicating increased hydrogen bonding involving catechol groups. Additionally, the intensified bending of the secondary amide at 1560 cm^{-1} and the appearance of a signal indicative of aromatic C−H stretching around 3000 cm^{-1} further confirmed the structure of HA-Cat.[18] A broad peak denoting the presence of aromatic C−C bonds was observed at 1652 cm^{-1}.

HA-Cat-Al was obtained by oxidation of the hydroxyl groups of HA-Cat using $NaIO_4$ as an oxidant agent (Figure 1A). The ^{1}H NMR spectrum of HA-Cat-Al exhibited an additional chemical shift between 5.28 and 4.82 ppm (Figure S2), and the ATR-FTIR spectrum displayed a distinct peak at 1735 cm^{-1} corresponding to the C═O bonds of the aldehyde groups (Figure S3).[19]

Previous data have shown that oxidation can result in the reduction of HA MW[20] and/or modification of the catechol groups to quinone. Indeed, GPC analysis confirms the cleavage of HA chains that was most pronounced in the case of HA with the highest MW (Table 1). The oxidation of catechol to quinone can be analyzed by UV−vis spectroscopy: characteristic broad intense bands appear in the region 336−380 nm of the quinone spectrum. The UV−vis spectra of HA-Cat-Al have a peak at 280 nm (Figure S4), corresponding to the vibration of the aromatic rings within the catechol groups[27−29] and lack any peaks above 300 nm, indicating no oxidation of catechol to quinone.[21] The peak at 280 nm was used to calculate the degree of substitution for HA-Cat-Al, which was 5.0%, 5.6%, and 3.7% for the derivatives obtained from HA with MW of 37, 454, and 926 kDa, respectively.

Table 1. Data about the Used Hydrogels' Components and Their Designation[a]

HA	HA-Cat-Al		HA-ADH	
MW (kDa)	MW (kDa)	DS (%)	MW (kDa)	hydrogel designation
926	42	3.7	786	HA_{828}-Cat
454	213	5.6	400	HA_{613}-Cat
37	36	5.0	48	HA_{84}-Cat

[a]MW values of the commercial HA and the respective derivatives were determined by gel permeation chromatography (GPC). The degree of substitution was determined from the UV-vis spectra. Hydrogels were generated by mixing components obtained from HA with the same MW.

HA-Al was synthesized by oxidizing HA (Figure 1B). Both ^{1}H NMR and ATR-FTIR spectroscopies confirmed the oxidation, showing additional chemical shifts between 5.28 and 4.82 ppm (Figure S2) and the appearance of a distinct peak at 1735 cm^{-1} (Figure S5), corresponding to the formation of new C═O bonds.

Lastly, HA-ADH was prepared through a carbodiimide-mediated coupling of ADH to the carboxyl groups of HA (Figure 1C). The methylene protons of ADH appear at δ = 1.70, 2.24, and 2.42 ppm in the ^{1}H NMR spectrum of HA-ADH (Figure S6). ATR-FTIR spectroscopy corroborated the successful modification; the stretching vibrations of the carbonyl groups (C═O) in the formed amide appear at 1650 cm^{-1} in the spectrum of HA-ADH. Additionally, signals associated with the hydrazide functional groups (−NHNH$_2$) can be observed at the 3350 cm^{-1} region, and peaks corresponding to the C═O stretching vibrations of the carboxyl groups are visible in the region of 1720 cm^{-1} (Figure S7).

3.2. Preparation of Hydrogels. The HA-Cat hydrogels were generated by the formation of a hydrazone covalent bond between the terminal amine group of HA-ADH and the aldehyde group of HA-Cat-Al or HA-Al (Figure 1D). We have tested different ratios between the components (Figure S8) and found that the 1:1 ratio was optimal as the hydrogels obtained at these conditions had superior mechanical properties. The obtained hydrogels are designated as HA_{828}-Cat, HA_{613}-Cat, and HA_{84}-Cat, where 828, 613, and 85 correspond to the sum between the MW of the HA-Cat-Al and HA-ADH (Table 1).

All HA-Cat hydrogels exhibited a rapid gelation, occurring within 3 to 60 min after the mixture of the HA-Cat-Al and the HA-ADH (Figure S9). Notably, hydrogels with higher MW (HA_{828}-Cat) displayed the fastest gelation (3 min), while those with lower MW (HA_{84}-Cat) exhibited a slower gelation process (60 min).

3.3. Hydrogels Characterization. The stability of hydrogels under physiological conditions is crucial for an effective transport of bioactive substances or support to tissue growth/regeneration over an extended period of time. Thus, we assessed the stability of the obtained hydrogels at 37 °C in PBS and in DMEM-F12 medium. HA_{84}-Cat hydrogels dissolved after 2 days of immersion in either PBS or medium (Figure S10), while the HA_{613}-Cat and HA_{828}-Cat hydrogels dissolved after 5 days.

To prevent the rapid dissolution of the hydrogels, a freeze-drying procedure was applied to enhance hydrogel stability by eliminating water content (Figure 2).[22,23] Therefore, all of the mechanical characterization and biological assays were performed with hydrated freeze-dried hydrogels. Considering the low stability exhibited by the HA_{84}-Cat hydrogel shortly after immersion in PBS or culture medium, we excluded this hydrogel from further investigation.

The HA-Cat and HA hydrogels were visually different (Figure 2): the HA-Cat was brownish, while the HA ones were white. This brownish color is due to the catechol brown pigmentation, related with complexation reactions that alter the catechol structure and lead to light absorption at the brown spectra of the wavelengths.[24]

The freeze-dried hydrogels were immersed in PBS for 14 days at 37 °C (Figure S11), and the measurements were taken

https://doi.org/10.1021/acs.biomac.3c01186
Biomacromolecules XXXX, XXX, XXX−XXX

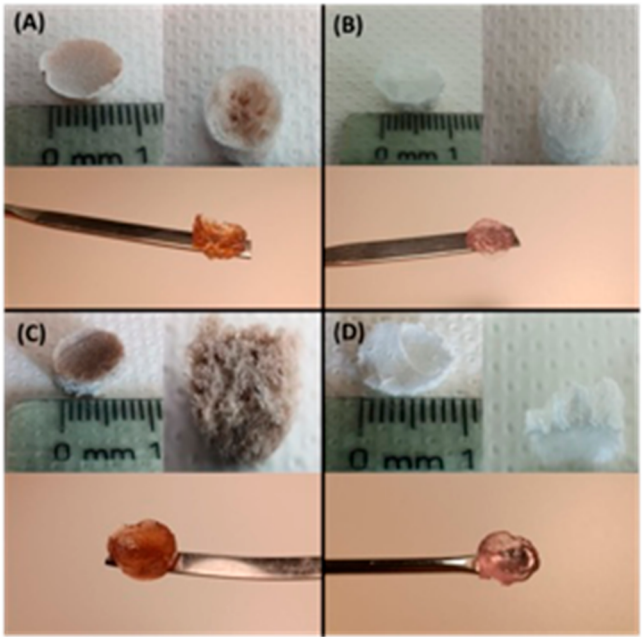


Figure 2. Macroscopic images of freeze-dried (up) and hydrated (DMEM-F12, down) hydrogels: (A) HA_{828}-Cat, (B) HA_{828}, (C) HA_{613}-Cat, and (D) HA_{613}.

on days 1, 3, 7 and 14, aiming to follow the dynamics and extent of swelling to a point at which the swelling process reaches equilibrium. Initially, HA_{828}-Cat and HA_{613}-Cat hydrogels exhibited substantial swelling, with a weight increase of 2361% for HA_{828}-Cat and 2245% for HA_{613}-Cat. However, after 3 days of immersion, HA_{828}-Cat attained equilibrium, while HA_{613}-Cat reached equilibrium after 7 days and had the highest swelling ability, i.e., a weight increase of 3446% was measured by day 14 for this hydrogel.

The stability of the hydrogels was investigated *in vitro* by monitoring the weight loss percentage during incubation in PBS (Figure 3A,B) and in DMEM-F12 (Figure 3C,D) at 37 °C. After 1 day of immersion in PBS, the weight loss of the

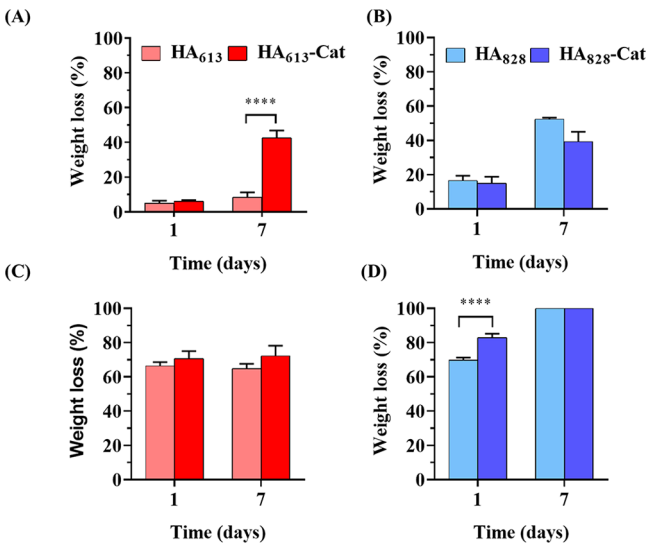


Figure 3. Data for the stability (represented as weight loss) of HA_{613}-Cat, HA_{613}, HA_{828}-Cat, and HA_{828} hydrogels in (A, B) PBS and (C, D) DMEM-F12 medium.

HA_{613}-Cat hydrogel was 6.2% ± 0.5% relative to its initial weight. The weight loss of respective control, i.e., HA_{613} hydrogel, for the same period was similar (5.0% ± 1.2%). After 7 days of immersion, a more substantial mass loss was observed for the HA_{613}-Cat hydrogel (42.7% ± 3.3%) than for the HA_{613} hydrogel (8.5% ± 2.5%). HA_{828}-Cat and HA_{828} hydrogels lose more mass after 1 day of immersion in PBS (15.0% ± 3.8% and 16.7% ± 2.7%, respectively) when compared to HA_{613}-Cat and HA_{613} hydrogels. At day 7, HA_{828}-Cat hydrogels had a similar weight loss (39.4% ± 5.6%) to HA_{613}-Cat hydrogel, while the respective catechol-free hydrogel lost significantly more weight (52.4% ± 0.9%).

Altogether, these data showed that the properties of the HA_{613}-Cat hydrogels align well with our aim to design an adhesive material with regenerative potential that can also serve as a vehicle for sustained drug release.

The stability of the hydrogels was also assessed in DMEM-F12 medium (used also in cellular assays). The change in the medium affected the stability profile, and the weight loss was significantly higher since the first day, but maintained stability until the seventh day of the assay: HA_{613}-Cat and HA_{613} hydrogels lost around 72.3% ± 5.9% and 64.8% ± 2.8%, respectively, of their weight. Similar profiles were observed for HA_{828} analogues: fast degradation during the first day with 82.9% ± 1.9% and 69.90% ± 1.12% of weight lost for HA_{828}-Cat and HA_{828} hydrogels, respectively. By the seventh day, the hydrogels vanished, showing that the HA_{828} hydrogels were not suitable for the intended application. The limited stability of HA_{828}-Cat and HA_{828} hydrogels can be explained by the lower MW of HA-Cat-Al (42 kDa) used as a component of these hydrogels, resulting in the formation of less hydrazone bonds compared to HA_{613}-Cat hydrogels.

Other essential properties of the developed hydrogels are their mechanical properties, including elasticity, rigidity, and resistance, which can influence cell behavior.[25] Hydrated freeze-dried hydrogels were characterized by rheology and DMA measurements.

In rheology, the hydrogel is subjected to minor deformations typically through small-amplitude oscillatory shear force, and two parameters are measured: the strain energy stored, known as the modulus of elasticity or stiffness (G'), and the loss modulus (G''), which represents the viscous behavior of the material and indicates how much energy is dissipated as heat within the material during the deformation process. Hydrogels have higher elasticity when $G' > G''$ or higher viscosity when $G'' > G'$.[26] The hydrogels developed herein exhibited stability up to a frequency of 10 rad/s (Figure 4A,B). Up to this frequency, the hydrogels had $G' > G''$, indicating that they reside in a solid state with superior elasticity. The G' of HA_{613}-Cat varied between 11.70 and 33.43 kPa and the G' of HA_{613} hydrogel was in the range 13.17−16.27 kPa, i.e., both hydrogels have mechanical properties that are suitable for SCI applications.

DMA is a nondestructive technique that is used to characterize the mechanical and viscoelastic properties under dynamic conditions. The storage modulus (E') is a measure of the stiffness of the sample and the loss factor (tan δ), defined as the ratio between dissipated energy and stored energy, provides information about the damping capacity.[27−29] The results showed the highest stiffness for HA_{613} and HA_{613}-Cat hydrogels with E' between 16 and 20 kPa and the lowest $E' < 5$ kPa for HA_{828} (Figure 4C). The analysis at various frequencies

https://doi.org/10.1021/acs.biomac.3c01186
Biomacromolecules XXXX, XXX, XXX−XXX

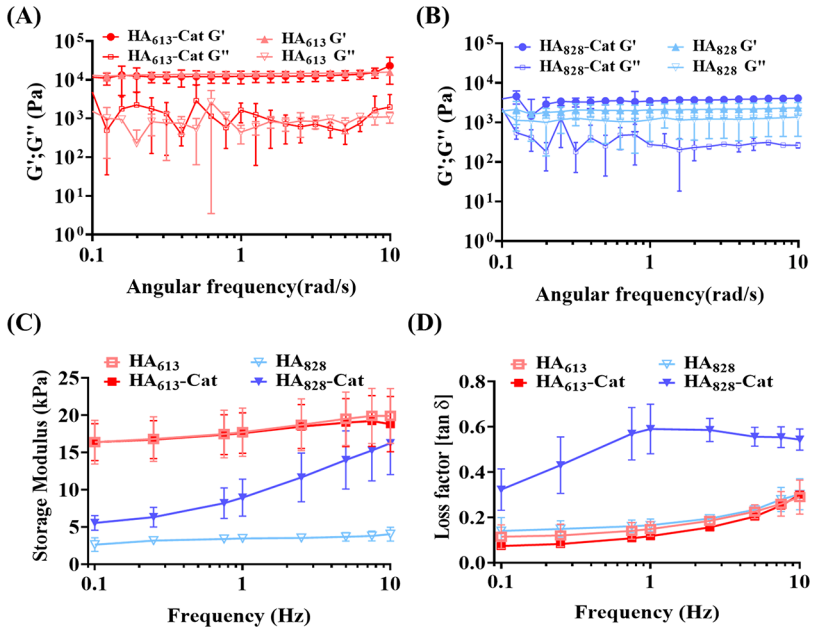


Figure 4. Mechanical properties of HA_{613}-Cat, HA_{613}, HA_{828}-Cat, and HA_{828} hydrogels: (A, B) oscillatory rheology data for different hydrogels showing the G' and G'' variation as a function of the frequency. Dynamic mechanical analysis (DMA) data for (C) storage modulus and (D) loss factor. The analysis was performed in DMEM-F12 medium.

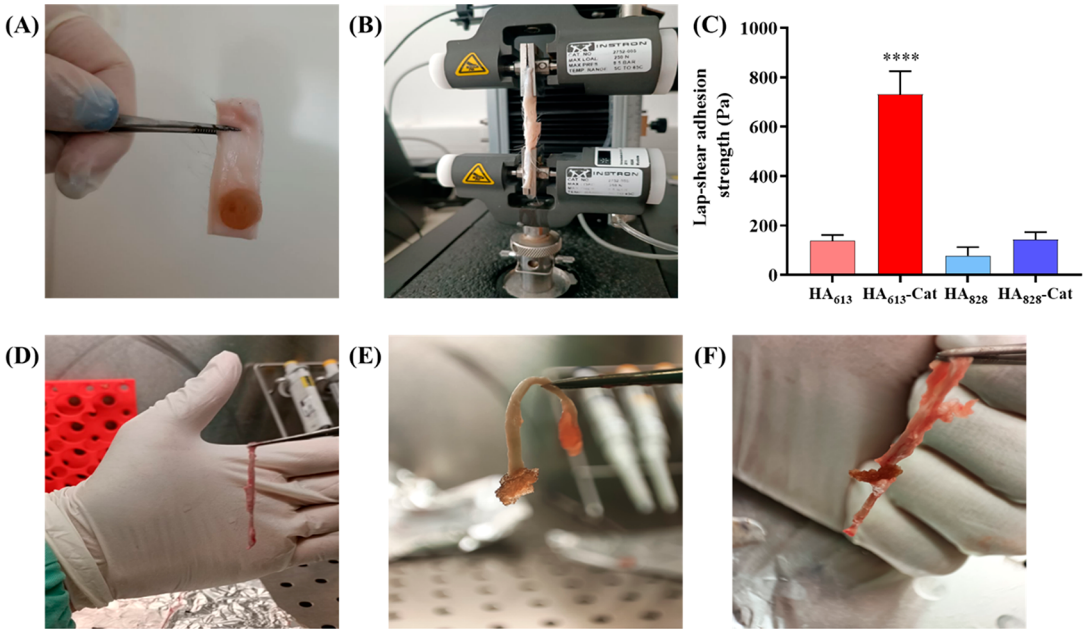


Figure 5. (A) Freeze-dried hydrogels adhered to porcine skin; (B) Set up used for lap-shear adhesion strength tests and (C) the results obtained from these tests.Significant differences are denoted with $p < 0.0001$(****). (D) Adhesion test on rat spinal cord; (E) Freeze-dried hydrogels adhered to rat spinal cord; (F) Adhesion test on two segments of the rat spinal cord.

revealed an increase of E' and tan δ with rising frequency, i.e., typical behavior of viscoelastic materials (Figure 4D).

An examination of the data collected at 1 Hz (frequency of the standing human body during unidirectional movement) showed that the HA_{613}-Cat and HA_{613} hydrogels had similar dynamic mechanical performance.[30] In summary, the DMA results showed that HA_{613}-Cat and HA_{613} hydrogels exhibit mechanical properties closer to the *ex vivo* spinal cord (E' = 5–15 kPa).[31]

Adhesiveness is an advantage for an implantable biomaterial because it implies a single intervention that places the biomaterial at the injured site, where it will adhere without displacement or migration to other body areas.[32] To determine the impact of catechol groups on the adhesive properties of hydrogels, a lap-shear adhesion test was performed under simulated physiological conditions. The hydrogels were hydrated in DMEM-F12 medium and placed between two overlapping pieces of porcine skin, pressed, and left immersed in PBS solution at 37 °C for 2 h (Figure 5A,B). The results showed that the HA_{613}-Cat hydrogel had significantly superior adhesive properties compared to the other hydrogels (Figure 5C). The enhanced adhesive properties of HA_{613}-Cat in

https://doi.org/10.1021/acs.biomac.3c01186
Biomacromolecules XXXX, XXX, XXX−XXX

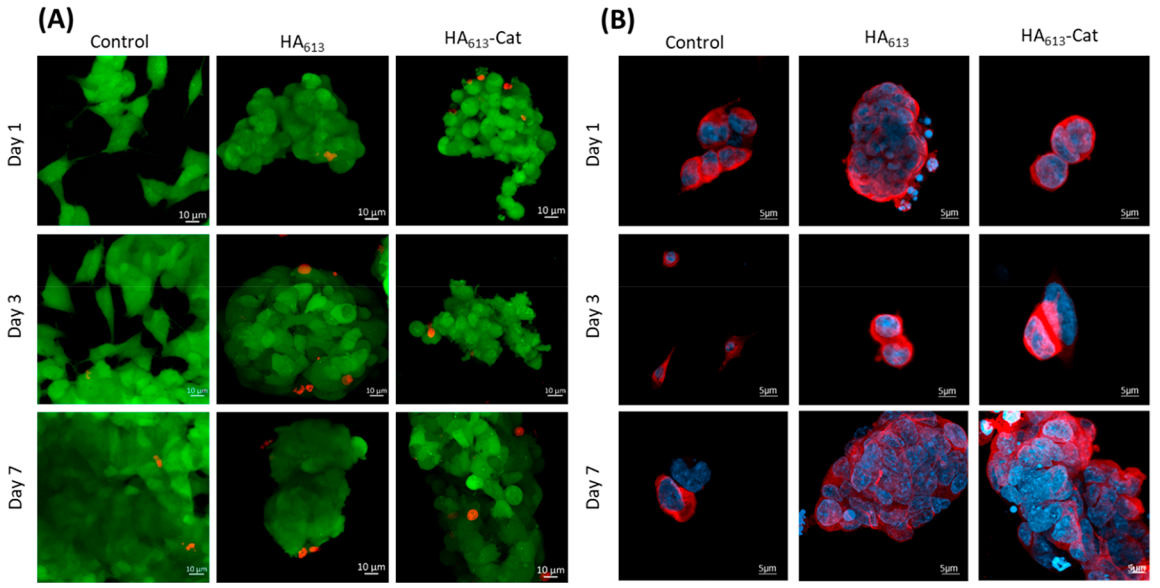


Figure 6. (A) Representative fluorescence microscopy images of the live/dead assay after 1, 3, and 7 days of SH-SY5Y culture on HA_{613}-Cat and HA_{613} hydrogels. Live cells (green) were stained with Calcein AM, while dead cells (red) were stained with propidium iodide. The scale bar is 10 μm. (B) Fluorescence microscopy images of SH-SY5Y cells cultured on the studied hydrogels and control TCPS. The cells were immunolabeled with anti-β-tubulin III (red) and the cell nuclei were stained with DAPI (blue). The scale bar is 5 μm.

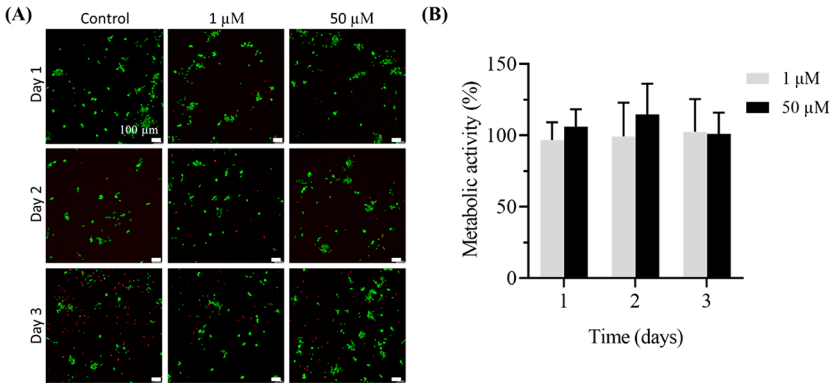


Figure 7. (A) Confocal microscopy images of SH-SY5Y cultures supplemented with ibuprofen at different concentrations (Control represents culture conditions without ibuprofen); Live cells (green) were stained with calcein AM, while dead cells (red) were stained with propidium iodide. The scale bar is 100 μm. (B) Metabolic activity (Alamar-blue assay) of SY-SY5Y cultures supplemented with ibuprofen; Data were normalized to the control (0 μM ibuprofen, 100% metabolic activity).

comparison to the HA_{823}-Cat hydrogel are due to the higher degree of substitution in the precursor HA-Cat-Al (Table 1, DS of 5.6 for HA_{613}-Cat vs 5.0 for HA_{823}-Cat), i.e., this hydrogel has more catechol moieties. The results suggest that the functionalization with catechol groups strengthens the contact between the HA_{613}-Cat hydrogel and the tissue, and thus, it is expected that these hydrogels can enhance wound healing following a SCI.

To confirm this hypothesis, a segment of the rat spinal cord was cut, and HA_{613}-Cat hydrogel was applied to glue the obtained tissue parts. The hydrogel adhered to the spinal cord (Figure 5D−F and Video S1) and enabled the glued tissue to endure the force of gravity. On the other hand, the control HA_{613} hydrogels were not able to adhere to the rat spinal cord (Video S2). These results showcase the efficacy of catechol functionalization in enhancing the bioadhesive properties of the hydrogels and highlight the potential application of the HA_{613}-Cat hydrogel in SCI treatment.

3.4. Cellular Studies. Keeping in mind the intended application of SCI treatment, we selected SH-SY5Y cells as a model for neural cells. The live/dead assay demonstrated that, after 7 days of culture, the HA_{613}-Cat and HA_{613} hydrogels supported high cell viability: only a few dead cells were seen on the hydrogels (Figure 6A).

The organization and differentiation of SY-SY5Y cells seeded on the hydrogels were analyzed using an antibody against β-Tubulin III (an early marker for neuronal differentiation) and DAPI (Figure 6B). SH-SY5Y cells seeded on hydrogels and TCPS (positive control) expressed β-Tubulin III on the first day of culture. Typical neuroblast-like morphology was observed with the adherent cells having nonpolarized cell bodies with some processes. The cells grew in clusters, and the size of these clusters increased over time for the hydrogel substrates (7 days of culture), but not for the control group.

Ibuprofen is a nonsteroidal anti-inflammatory drug commonly used to reduce pain, inflammation, and other symptoms related to traumatic injuries. Recent research indicates that

https://doi.org/10.1021/acs.biomac.3c01186
Biomacromolecules XXXX, XXX, XXX−XXX

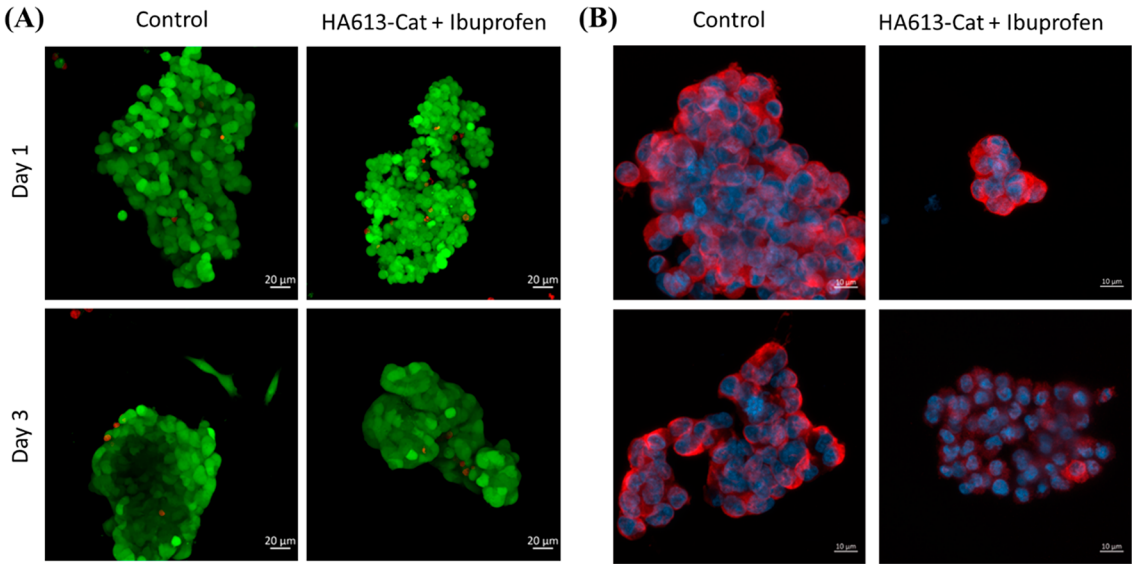


Figure 8. (A) Confocal microscopy images showing cell viability (live/dead assay) after 1 and 3 days of SH-SY5Y culture in contact with tissue culture polystyrene (TCPS, control) and HA_{613}-Cat hydrogel with ibuprofen. Live cells are stained in green, and dead cells are visible in red. The scale bar is 20 μm. (B) Fluorescence microscopy images of SH-SY5Y cells seeded on control TCPS and HA_{613}-Cat hydrogel loaded with ibuprofen: the cells were immunolabeled with β-tubulin III (red) and stained with DAPI (blue) for visualization of the nuclei. The scale bar is 10 μm.

ibuprofen might enhance corticospinal axons' regeneration after SCI.[33] Therefore, ibuprofen was encapsulated in the hydrogels.

Before encapsulation, the cytotoxicity of ibuprofen on SH-SY5Y cells was assessed at different concentrations for 3 days. This period was chosen because previous studies using similar systems have shown that ibuprofen is released within the initial 72 h.[34] It was also reported that ibuprofen exhibits minimal cytotoxicity at a concentration of 100 μM.[6] Consequently, we investigated its cytotoxicity at two distinct concentrations below this limit, namely, 1 and 50 μM. The live/dead assay (Figure 7A) demonstrated similar cell viability over the 3 days for both concentrations and for the control group (without ibuprofen). The results for the cell metabolic activity agree with the live/dead data and show that ibuprofen is not cytotoxic for SH-SY5Y cells at concentrations up to 50 μM (Figure 7B).

Ibuprofen was encapsulated in HA_{613}-Cat hydrogel at a concentration of 50 μM. The live/dead assay of SH-SY5Y cells cultured on the loaded hydrogels for 1 and 3 days (Figure 8A) showed viable cells and were compared with the control conditions (no ibuprofen), i.e., the loaded ibuprofen did not affect cell viability.

The analysis of SY-SY5Y cell morphology and organization after 1 day of culture on the control TCPS and HA_{613}-Cat hydrogel loaded with ibuprofen showed a rounded cellular shape for both materials (Figure 8B). These findings provide clear evidence that the developed hydrogels, incorporating ibuprofen, do not hinder cell growth.

4. CONCLUSIONS

In this study, we reported the synthesis and characterization of mussel-inspired HA hydrogel hydrazone bonds between two HA derivatives with complementary chemistry. This chemical cross-linking is catalytic-free, chemoselective, instantaneous, and nonreversible under physiological conditions. The functionalization with catechol groups provided crucial enhancement of hydrogels' adhesive properties, as demonstrated through experimental assays conducted with porcine skin and rat spinal cord. The obtained hydrogels had no adverse effects on SH-SY5Y cells and up-regulated specific neuronal marker β-III tubulin. Moreover, the hydrogels can be used as vesicles for the delivery of anti-inflammatory drugs, thus, exhibiting unique advantages for SCI treatment.

■ ASSOCIATED CONTENT

Supporting Information

The Supporting Information is available free of charge at https://pubs.acs.org/doi/10.1021/acs.biomac.3c01186.

GPC analysis of HA with different MW (Figure S1); ^{1}H NMR spectra of HA derivatives with catechol and aldehyde groups (Figure S2); ATR-FTIR spectra of HA, HA-Cat, and HA-Cat-Al (Figure S3); UV−vis spectra of HA-Cat-Al derivatives with different MWs (Figure S4); ATR-FTIR spectrum of HA-Al (Figure S5); ^{1}H NMR spectrum of HA modified with ADH (Figure S6); ATR-FTIR spectrum of HA-ADH (Figure S7); Oscillatory rheology data for different HA-Cat-Al: HA-ADH ratios with different HA MWs (Figure S8); Macroscopic appearance of HA-Cat hydrogels before freeze-drying process (Figure S9); Visual assessment of the stability of HA-Cat hydrogels (Figure S10); Results for the swelling of the hydrogels (Figure S11) (PDF)

Video S1: Adhesion test of HA-Cat hydrogels on rat spinal cord (MP4)

Video S2: Adhesion test of HA hydrogels on rat spinal cord (MP4)

■ AUTHOR INFORMATION

Corresponding Authors

Daniela Peixoto − *3B's Research Group, I3Bs − Research Institute on Biomaterials, Biodegradables and Biomimetics, University of Minho, Headquarters of the European Institute of Excellence on Tissue Engineering and Regenerative Medicine, 4805-017 Barco/Guimarães, Portugal; ICVS/3B's−PT Government Associate Laboratory, 4710-057*

https://doi.org/10.1021/acs.biomac.3c01186
Biomacromolecules XXXX, XXX, XXX−XXX

Braga/Guimarães, Portugal; Email: daniela.peixoto@i3Bs.uminho.pt

Natália M. Alves − *3B's Research Group, I3Bs − Research Institute on Biomaterials, Biodegradables and Biomimetics, University of Minho, Headquarters of the European Institute of Excellence on Tissue Engineering and Regenerative Medicine, 4805-017 Barco/Guimarães, Portugal; ICVS/3B's−PT Government Associate Laboratory, 4710-057 Braga/Guimarães, Portugal;* orcid.org/0000-0002-8741-4091; Email: nalves@i3Bs.uminho.pt

Authors

Diogo Duarte − *3B's Research Group, I3Bs − Research Institute on Biomaterials, Biodegradables and Biomimetics, University of Minho, Headquarters of the European Institute of Excellence on Tissue Engineering and Regenerative Medicine, 4805-017 Barco/Guimarães, Portugal; ICVS/3B's−PT Government Associate Laboratory, 4710-057 Braga/Guimarães, Portugal*

Cátia Correia − *3B's Research Group, I3Bs − Research Institute on Biomaterials, Biodegradables and Biomimetics, University of Minho, Headquarters of the European Institute of Excellence on Tissue Engineering and Regenerative Medicine, 4805-017 Barco/Guimarães, Portugal; ICVS/3B's−PT Government Associate Laboratory, 4710-057 Braga/Guimarães, Portugal*

Rui L. Reis − *3B's Research Group, I3Bs − Research Institute on Biomaterials, Biodegradables and Biomimetics, University of Minho, Headquarters of the European Institute of Excellence on Tissue Engineering and Regenerative Medicine, 4805-017 Barco/Guimarães, Portugal; ICVS/3B's−PT Government Associate Laboratory, 4710-057 Braga/Guimarães, Portugal;* orcid.org/0000-0002-4295-6129

Iva Pashkuleva − *3B's Research Group, I3Bs − Research Institute on Biomaterials, Biodegradables and Biomimetics, University of Minho, Headquarters of the European Institute of Excellence on Tissue Engineering and Regenerative Medicine, 4805-017 Barco/Guimarães, Portugal; ICVS/3B's−PT Government Associate Laboratory, 4710-057 Braga/Guimarães, Portugal;* orcid.org/0000-0001-6818-3374

Complete contact information is available at: https://pubs.acs.org/10.1021/acs.biomac.3c01186

Author Contributions

[§]These authors contributed equally to this work (D.D. and C.C.).

Notes

The authors declare no competing financial interest.

■ ACKNOWLEDGMENTS

The authors would like to thank the contributions to this research from the Project "TERM RES Hub − Scientific Infrastructure for Tissue Engineering and Regenerative Medicine", Reference PINFRA/22190/2016 (Norte-01-0145-FEDER-022190), funded by the Portuguese National Science Foundation (FCT) through the OE component in cooperation with the Northern Portugal Regional Coordination and Development Commission (CCDR-N), for providing relevant lab facilities, state-of-the-art equipment, and highly qualified human resources, and the FCT and European Program FEDER/FEEI for the financial support through the project. The authors acknowledge funding by the European Union's Research and Innovation Programme Grant Agreements 101008041 (Project SHIFT) and HORIZON-EIC-2022-PATHFINDEROPEN-01-101099063 (Project Aptadegrad). FCT is also acknowledged for the Ph.D. scholarship SFRH/BD/143209/2019 granted to C.C.

■ REFERENCES

(1) Alizadeh, A.; Dyck, S. M.; Karimi-Abdolrezaee, S. Traumatic Spinal Cord Injury: An Overview of Pathophysiology, Models and Acute Injury Mechanisms. *Front. Neurol.* **2019**, *10*, 1−25.

(2) Bennett, J.; Das, J. M.; Emmady, P. D. *Spinal Cord Injuries*; StatPearls Publishing: Treasure Island, FL, 2022.

(3) Alizadeh, A.; Dyck, S. M.; Karimi-Abdolrezaee, S. Traumatic Spinal Cord Injury: An Overview of Pathophysiology, Models and Acute Injury Mechanisms. *Front. Neurol.* **2019**, *10*, 282.

(4) Costăchescu, B.; Niculescu, A. G.; Dabija, M. G.; Teleanu, R. I.; Grumezescu, A. M.; Eva, L. Novel Strategies for Spinal Cord Regeneration. *Int. J. Mol. Sci.* **2022**, *23* (9), 4552.

(5) Anjum, A.; Yazid, M. D.; Fauzi Daud, M.; Idris, J.; Ng, A. M. H.; Selvi Naicker, A.; Ismail, O. H. R.; Athi Kumar, R. K.; Lokanathan, Y. Spinal Cord Injury: Pathophysiology, Multimolecular Interactions, and Underlying Recovery Mechanisms. *Int. J. Mol. Sci.* **2020**, *21* (20), 7533.

(6) Zhang, Y.; Anoopkumar-Dukie, S.; Mallik, S. B.; Davey, A. K. SIRT1 and SIRT2Modulators Reduce LPS-Induced Inflammation in HAPI Microglial Cells and Protect SH-SY5Y Neuronal Cells in Vitro. *J. Neural. Transm.* **2021**, *128* (5), 631−644.

(7) Jensen, G.; Holloway, J. L.; Stabenfeldt, S. E. Hyaluronic Acid Biomaterials for Central Nervous System Regenerative Medicine. *Cells* **2020**, *9* (9), 2113.

(8) Kim, J.; Lee, C.; Ryu, J. H. Adhesive Catechol-conjugated Hyaluronic Acid for Biomedical Applications: A Mini Review. *Appl. Sci.* **2021**, *11* (1), 21.

(9) Zhang, H.; Xiao, Y.; Chen, P.; Cao, H.; Bai, W.; Yang, Z.; Yang, P.; Li, Y.; Gu, Z. Robust Natural Polyphenolic Adhesives against Various Harsh Environments. *Biomacromolecules* **2022**, *23* (8), 3493−3504.

(10) Xu, Y.; Hu, J.; Hu, J.; Cheng, Y.; Chen, X.; Gu, Z.; Li, Y. Bioinspired Polydopamine Hydrogels: Strategies and Applications. *Prog. Polym. Sci.* **2023**, *146*, No. 101740.

(11) Zhang, X.; Li, Z.; Yang, P.; Duan, G.; Liu, X.; Gu, Z.; Li, Y. Polyphenol Scaffolds in Tissue Engineering. *Mater. Horiz.* **2021**, *8*, 145−167.

(12) Lee, Y.; Chung, H. J.; Yeo, S.; Ahn, C. H.; Lee, H.; Messersmith, P. B.; Park, T. G. Thermo-Sensitive, Injectable, and Tissue Adhesive Sol-Gel Transition Hyaluronic Acid/Pluronic Composite Hydrogels Prepared from Bio-Inspired Catechol-Thiol Reaction. *Soft. Matter.* **2010**, *6* (5), 977−983.

(13) Hozumi, T.; Kageyama, T.; Ohta, S.; Fukuda, J.; Ito, T. Injectable Hydrogel with Slow Degradability Composed of Gelatin and Hyaluronic Acid Cross-Linked by Schiff's Base Formation. *Biomacromolecules* **2018**, *19* (2), 288−297.

(14) Luo, Y.; Kirker, K. R.; Prestwich, G. D. Cross-Linked Hyaluronic Acid Hydrogel Films: New Biomaterials for Drug Delivery. *J. Controlled Release* **2000**, *69* (1), 169−184.

(15) Zhang, L.; Liu, L.; Qian, Y.; Chen, Y. The Effects of Cryoprotectants on the Freeze-Drying of Ibuprofen-Loaded Solid Lipid Microparticles (SLM). *Eur. J. Pharm. Biopharm.* **2008**, *69* (2), 750−759.

(16) Li, K.; Zan, X.; Tang, C.; Liu, Z.; Fan, J.; Qin, G.; Yang, J.; Cui, W.; Zhu, L.; Chen, Q. Tough, Instant, and Repeatable Adhesion of Self-Healable Elastomers to Diverse Soft and Hard Surfaces. *Adv. Sci.* **2022**, *9* (12), 1−13.

(17) Zhang, J.; Hu, Y.; Zhang, L.; Zhou, J.; Lu, A. Transparent, Ultra-Stretching, Tough, Adhesive Carboxyethyl Chitin/Polyacrylamide Hydrogel Toward High-Performance Soft Electronics. *Nano-micro. Lett.* **2023**, *15* (1), 1−22.

(18) Pornpitchanarong, C.; Rojanarata, T.; Opanasopit, P.; Ngawhirunpat, T.; Patrojanasophon, P. Catechol-Modified Chitosan/Hyaluronic Acid Nanoparticles as a New Avenue for Local Delivery of Doxorubicin to Oral Cancer Cells. *Colloids. Surf. B* **2020**, *196*, No. 111279.
(19) Dahlmann, J.; Krause, A.; Möller, L.; Kensah, G.; Möwes, M.; Diekmann, A.; Martin, U.; Kirschning, A.; Gruh, I.; Dräger, G. Fully Defined in Situ Cross-Linkable Alginate and Hyaluronic Acid Hydrogels for Myocardial Tissue Engineering. *Biomater.* **2013**, *34* (4), 940−951.
(20) Pandit, A. H.; Mazumdar, N.; Ahmad, S. Periodate Oxidized Hyaluronic Acid-Based Hydrogel Scaffolds for Tissue Engineering Applications. *Int. J. Biol. Macromol.* **2019**, *137*, 853−869.
(21) Lan, Y. T.; Cheng, Q. P.; Xu, J.; Lin, S. H.; Lin, J. M.; Hsu, S. H. Gelation and the Self-Healing Behavior of the Chitosan−Catechol Hydrogel. *Polymers (Basel)* **2022**, *14* (21), 4614.
(22) Sornkamnerd, S.; Okajima, M. K.; Kaneko, T. Tough and Porous Hydrogels Prepared by Simple Lyophilization of LC Gels. *ACS Omega* **2017**, *2* (8), 5304−5314.
(23) Annabi, N.; Nichol, J. W.; Zhong, X.; Ji, C.; Koshy, S.; Khademhosseini, A.; Dehghani, F. Controlling the Porosity and Microarchitecture of Hydrogels for Tissue Engineering. *Tissue Eng. Part B. Rev.* **2010**, *16* (4), 371−383.
(24) Chin, H.; Hopstock, K. S.; Fleming, L. T.; Nizkorodov, S. A.; Al-Abadleh, H. A. Effect of Aromatic Ring Substituents on the Ability of Catechol to Produce Brown Carbon in Iron(III)- Catalyzed Reactions. *Environ. Sci. Atmos.* **2021**, *1* (2), 64−78.
(25) Chan, B. P.; Leong, K. W. Scaffolding in Tissue Engineering: General Approaches and Tissue-Specific Considerations. *Eur. Spine J.* **2008**, *17*, 467−479.
(26) Yan, C.; Pochan, D. J. Rheological Properties of Peptide-Based Hydrogels for Biomedical and Other Applications. *Chem. Soc. Rev.* **2010**, *39* (9), 3528−3540.
(27) Mano, J. F. Viscoelastic Properties of Chitosan with Different Hydration Degrees as Studied by Dynamic Mechanical Analysis. *Macromol. Biosci.* **2008**, *8* (1), 69−76.
(28) Correia, C.; Sousa, R. O.; Vale, A. C.; Peixoto, D.; Silva, T. H.; Reis, R. L.; Pashkuleva, I.; Alves, N. M. Adhesive and Biodegradable Membranes Made of Sustainable Catechol-Functionalized Marine Collagen and Chitosan. *Colloids Surf., B* **2022**, *213*, No. 112409.
(29) Caridade, S. G.; Merino, E. G.; Alves, N. M.; Bermudez, V. de Z.; Boccaccini, A. R.; Mano, J. F. Chitosan Membranes Containing Micro or Nano-Size Bioactive Glass Particles: Evolution of Biomineralization Followed by in Situ Dynamic Mechanical Analysis. *J. Mech. Behav. Biomed. Mater.* **2013**, *20*, 173−183.
(30) Loram, I. D.; Gawthrop, P. J.; Lakie, M. The Frequency of Human, Manual Adjustments in Balancing an Inverted Pendulum Is Constrained by Intrinsic Physiological Factors. *Physiol. J.* **2006**, *577* (1), 417−432.
(31) Bartlett, R. D.; Eleftheriadou, D.; Evans, R.; Choi, D.; Phillips, J. B. Mechanical Properties of the Spinal Cord and Brain: Comparison with Clinical-Grade Biomaterials for Tissue Engineering and Regenerative Medicine. *Biomater.* **2020**, *258*, No. 120303.
(32) Correia, C.; Reis, R. L.; Pashkuleva, I.; Alves, N. M. Adhesive and Self-Healing Materials for Central Nervous System Repair. *Biomater. Adv.* **2023**, *151*, No. 213439.
(33) Wang, X.; Budel, S.; Baughman, K.; Gould, G.; Song, K. H.; Strittmatter, S. M. Ibuprofen Enhances Recovery from Spinal Cord Injury by Limiting Tissue Loss and Stimulating Axonal Growth. *J. Neurotrauma* **2009**, *26* (1), 81−95.
(34) Mauri, E.; Rossetti, A.; Mozetic, P.; Schiavon, C.; Sacchetti, A.; Rainer, A.; Rossi, F. Ester Coupling of Ibuprofen in Hydrogel Matrix: A Facile One-Step Strategy for Controlled Anti-Inflammatory Drug Release. *Eur. J. Pharm. Biopharm.* **2020**, *146*, 143−149.

https://doi.org/10.1021/acs.biomac.3c01186
Biomacromolecules XXXX, XXX, XXX−XXX